Continuous Raman sideband cooling beyond the Lamb-Dicke regime in a trapped ion chain

Qiming Wu* and Yue Shi
Department of Physics, New York University, New York, New York 10003, USA

Jiehang Zhang†
School of Physical Sciences, University of Science and Technology of China, Hefei 230026, China;
Shanghai Research Center for Quantum Science and CAS Center for Excellence in Quantum Information and Quantum Physics, University of Science and Technology of China, Shanghai 201315, China;
and Hefei National Laboratory, University of Science and Technology of China, Hefei 230088, China

(Received 15 August 2022; accepted 5 January 2023; published 13 April 2023)

We report continuous Raman sideband cooling of a long ion chain close to the motional ground state beyond the Lamb-Dicke (LD) regime. By driving multiple sideband transitions simultaneously, we show that nearly all axial modes of a 24-ion chain are cooled to the ground state, with an LD parameter as large as $\eta = 1.3$, spanning a frequency bandwidth of 4 MHz. Compared to traditional ground-state cooling methods such as pulsed sideband cooling or electromagnetically-induced-transparency cooling, our method offers two key advantages: disposal of pulse optimization, and a wide bandwidth covering the entire spectrum. This technique contributes as a crucial step for large-scale quantum information processing with linear ion chains and higher dimensions alike, and can be readily generalized to other atomic and molecular systems.

DOI: 10.1103/PhysRevResearch.5.023022

I. INTRODUCTION

Trapped atomic ions are a leading platform for quantum computation and simulation [1–5], precision time keeping [6], and probing fundamental physics [7,8]. As a prime candidate for quantum information processing, trapped ions combine high-fidelity state preparation and detection [9], long coherence times [10], and high single- and two-qubit gate fidelities [9,11–13]. These ion qubits can either be coupled in the dispersive regime to realize a quantum simulator with long-range interactions [14–16] or controlled with optimized laser pulses to realize a digital quantum computer [1–3]. In both regimes, quantum entanglement is generated by phonon-mediated interactions, which require the motional states to be well defined to avoid incoherent thermal disturbances. Cooling of a trapped ion chain to the motional ground state hence serves as the starting point of high-fidelity quantum logic operations [11–13].

Resolved sideband cooling is a general method of cooling trapped particles to the quantum harmonic oscillator ground state. It has been demonstrated in various physical systems such as trapped ions [17–19], atoms in optical lattices [20,21], and tweezers [22,23]. In the case of ions, the conventional setting with tight confinement is referred to as the Lamb-Dicke regime (LDR) [24], in which the motional wavefunction of the ion is well localized and much smaller than the spatial gradient of the coupling electromagnetic wave. The coupling between the internal electronic and external motional states is weak enough that one can approximate the first-order sidebands as the dominant spin-phonon interaction. Concatenating pulsed red sideband (RSB) excitations and dissipative optical pumping processes [17], ground-state cooling can be achieved after iterating through different mean phonon numbers [25]. Despite its successful usage in single- and few-ion systems, generalizing this technique to long ion chains meets two crucial challenges: first, sequential cooling of all collective modes of the coupled harmonic oscillator system becomes slow as the system size increases [26], and second, certain motional modes such as the low-frequency axial modes of a linear chain occupy high phonon numbers, which is detrimental to entangling gates in both axial- and transverse-mode schemes [2,27]. Finally, sideband cooling beyond the LDR becomes nontrivial, where the coupling light is strongly modulated by the particle's motion and the cooling efficiency is limited by the large photon-recoil effects [28].

In the face of these challenges, various methods have been employed to improve the cooling efficiency and bandwidth. Coupling to higher-order sidebands allows faster cooling [23,29], at the expense of complicated pulse optimizations [25]. Electromagnetically-induced-transparency (EIT) cooling utilizes Fano-like resonances arising from laser-atom interactions to engineer coherent dark states for suppressing unwanted excitations [30–33]. EIT cooling with an improved bandwidth has been demonstrated for four ions [34]. However, the bandwidth is still limited by the atomic structure.

*qiming.wu@nyu.edu
†jzhang2022@ustc.edu.cn

The cooling scheme relies on the specific atomic levels, and cooling of ions with nuclear spin $I > 1/2$ has not yet been reported. Polarization gradient cooling serves as a fast intermediate step without cooling to the ground state [35–37], thus requiring further sideband cooling. While each method has respective advantages, a single-step technique that combines robustness, simplicity, low temperatures, and high bandwidth is highly desirable.

In order to perform information processing with a large ion crystal in a linear configuration, it is inevitable to have loose axial confinement, which leads to a high Lamb-Dicke (LD) parameter, especially for light ions. On the other hand, a high LD parameter finds many applications, such as enabling faster entangling operations [38–40], enhancing quantum sensing [41], and accelerating novel n-qubit quantum gates [42]. Solving the challenge of ground motional state preparation in the presence of a high LD parameter hence becomes an important prerequisite for these new applications. The case of beryllium ions (Be^+) well illustrates such a scenario: the light mass and clean atomic structure have enabled high-fidelity entangling gates [11] and large-scale quantum simulations [43], but for long linear chains with dozens of Be^+ ions, the axial modes can span over several megahertz of bandwidth with the largest LD parameters exceeding 1, making ground-state cooling for all modes challenging with existing methods.

In this article, we solve these challenges by presenting a continuous Raman sideband cooling (CRSC) scheme akin to that used in optical qubits [44]: we continuously drive multiple RSB transitions, and simultaneously apply weak pumping light to lower phonon occupancy and reset the qubits. In contrast to the pulsed regime, where a coherent step is followed by a dissipative step, our scheme cools on all phonon states simultaneously and can be thought of as a continuous quantum Zeno process [45] directed towards the motional ground state. The CRSC is also less susceptible to phonon state distribution and population trapping in certain number states with weak first-order sideband coupling [23]; thus, driving higher-order RSBs is not necessary for ground-state cooling even far outside the LDR. With this technique, we demonstrate cooling of a single ion to the ground state within 200 μs and efficient cooling of long linear chains containing up to 24 $^9Be^+$ ions, with LD parameters as large as $\eta = 1.3$, spanning a frequency bandwidth of 4 MHz.

II. EXPERIMENTAL SETUP

We perform this experiment with ion ablation loaded into a four-rod radio-frequency (RF) Paul trap [46] with a typical radial frequency of $\omega_x/2\pi = 3.3$ MHz and axial frequencies ranging from $\omega_z/2\pi = 270$ to 735 kHz. Figure 1(a) illustrates the experimental configuration: a σ_+-polarized Doppler beam near 313 nm is counteraligned with a 120 G magnetic field defining the quantization axis, with three tones providing Doppler cooling and state detection and two optical pumping frequencies. A pair of global Raman beams with waists of 270×21 μm^2 on the ion plane propagate at 45° with respect to the trap z axis, generating a momentum kick $\hbar\Delta\vec{k}$ along the axial direction. The Raman beam polarizations are tuned to be both linear, one parallel (π light) and one perpendicular (equal σ_+/σ_- light) to the magnetic field, minimizing the vector Stark shift for our Zeeman qubit operations [47]. Figure 1(b) shows the atomic energy levels of $^9Be^+$ involved in CRSC. We first apply Doppler cooling for 1 ms with stepwise reduced laser power to approach the Doppler limit ($\bar{n} \approx 6$–17 depending on the axial f requency), followed by initiating the ions on the $|\downarrow\rangle \equiv {}^2S_{1/2}|F = 2, m_F = 2\rangle$ state. During CRSC, Raman beams 280 GHz red-detuned from the $^2P_{3/2}$ excited state drive the $|\downarrow\rangle \leftrightarrow |\uparrow\rangle \equiv {}^2S_{1/2}|F = 1, m_F = 1\rangle$ transition, with the difference frequencies tuned to be on resonance with the red sidebands at a maximum two-photon carrier Rabi frequency of $\Omega_0/2\pi = 300$ kHz. We use an arbitrary waveform generator (AWG) for the RF signal modulating the laser frequencies, covering the entire motional spectrum with equal amplitudes on all other modes except twice the power on the center-of-mass (c.m.) mode. Meanwhile, we apply weak optical pumping beams to clear out the populations on the $|\uparrow\rangle$ and $|\text{aux}\rangle \equiv {}^2S_{1/2}|F = 2, m_F = 1\rangle$ states via the $|e\rangle \equiv {}^2P_{3/2}|m_I = 3/2, m_j = 1/2\rangle$ state, with Rabi frequencies of $\Omega_1/2\pi = 700$ kHz and $\Omega_2/2\pi = 600$ kHz, respectively (corresponding to saturation parameters $s = 0.23$ and 0.45). This pumping scheme eliminates the need for a D1 line laser, which further simplifies the beryllium quantum processor setup, requiring only one frequency-stabilized laser. After CRSC, we probe the RSB and blue sideband (BSB) transitions with coherent Raman operations, followed by state detection using spin-dependent fluorescence.

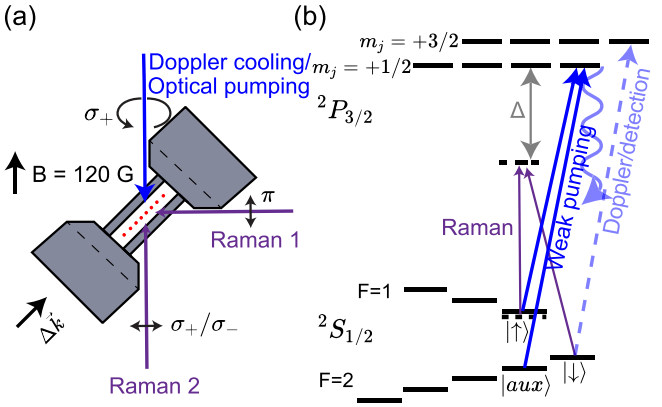

FIG. 1. Experimental setup and $^9Be^+$ atomic levels. (a) Ion trap and laser beam configurations: four-rod trap holds a linear chain under a 120 G magnetic field; a three-tone Doppler beam with a pure σ_+ polarization provides Doppler cooling, spin-state detection, and optical pumping. Raman 1 and 2 with π and $\sigma_\pm$ polarizations address the qubit transition with a differential momentum along the trap axial direction. (b) Atomic energy levels involved in the CRSC (not to scale). A pair of multitone Raman beams drive RSB transitions in parallel on the $|\downarrow\rangle \leftrightarrow |\uparrow\rangle$ transition, while weak pumping beams clear out the populations on the $|\uparrow\rangle$ and $|\text{aux}\rangle$ states through dissipation from the $^2P_{3/2}$ state (wavy line).

III. COOLING A SINGLE ION

We first show the ground cooling of the axial mode of a single ion with $\eta = 0.78$. After applying CRSC by driving the first-order RSB and optical pumping transitions, we measure the mean phonon number $\bar{n}$ with the ratio of red- to blue-sideband (BSB) amplitudes $R = P_{\text{rsb}}/P_{\text{bsb}} = \bar{n}/(\bar{n}+1)$

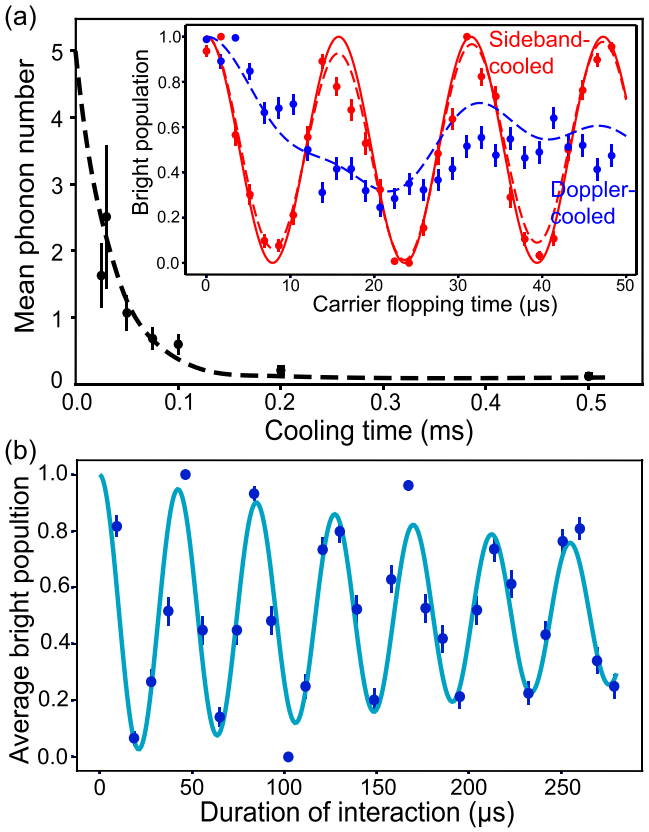

FIG. 2. Continuous sideband cooling with one and two ions. (a) Cooling dynamics of a single ion. Black points are the measured $\bar{n}$ with the sideband ratio method; error bars denote one standard deviation of the quantum projection noise, and the dashed black line is an exponential fit. Inset shows spin dynamics of carrier transition: red and blue points show the time evolution of spin after CRSC and with only Doppler cooling. The solid red line shows a sine fit to the data. Dashed red and blue lines show the numerical spin evolution with $\bar{n} = 0.1$ and 6, respectively. (b) Average spin excitation of two-ion crystal under the Mølmer-Sørensen interaction. The solid blue line is a fit of a sine function with an exponential decay envelope.

[48] at different sideband cooling durations τ_c [Fig. 2(a)]. An exponential fit shows a $1/e$ cooling time constant of 32 μs, with a steady-state $\bar{n} = 0.10(4)$ limited by the single photon recoil from optical pumping. Alternatively, we analyze the $\bar{n}$ with the carrier Rabi flopping of a single ion, which is strongly modulated even at low phonon occupations due to the large LD parameter. The spin evolution under a thermal state assumption is

$$P_e(t) = \frac{1}{2}\left[1 + \sum_{n=0}^{\infty} \frac{\bar{n}^n}{(\bar{n}+1)^{n+1}} \cos(\Omega_{n,n} t)\right], \qquad (1)$$

where $\Omega_{n,n}$ corresponds to the Rabi frequency of the carrier transition on the motional Fock state $|n\rangle$. The inset in Fig. 2(a) shows the carrier Rabi flopping of a single ion before and after CRSC: the spin coherence of a Doppler-cooled ion quickly disappears because of the thermal modulation, and the spin dynamics after ground-state cooling show coherent sinusoidal oscillations. While in pulsed sideband cooling, the thermal distribution assumption might be inaccurate [6,25]; in our scheme, the two methods for $\bar{n}$ analysis agree well despite the different sensitivities for the detailed distribution. We compare the experimental cooling dynamics with a numerical simulation using the master equation and find a good agreement of cooling to the ground state in 200 μs (see Appendix A.

We then implement cooling a pair of ions, serving as the first step towards generalizing to larger systems. During the CRSC, we apply dual RSBs on the c.m. ($\eta = 0.78$) and stretch ($\eta = 0.59$) modes with simultaneous optical pumping. After the cooling sequence, we drive Ising interactions between the two qubits off-resonantly using the bichromatic Mølmer-Sørensen scheme [38] and observe coherent dynamics with a $1/e$ decay time of 390 μs [Fig. 2(b)], exceeding the dominant dephasing from single Zeeman qubit T_2^* time of 300 μs (measured with a Ramsey sequence), manifesting dynamical decoupling effects due to the collective drive. To the best of our knowledge, this two-ion interaction is under the largest LD parameter reported so far, even exceeding that in ultrafast gates [39,40].

IV. COOLING AN EIGHT-ION CHAIN

We next study the cooling of an eight-ion chain. We program the AWG with eight tones to match the RSB frequencies of the axial vibrational modes. The mode LD parameters range between 0.33 and 0.78, from the highest to lowest

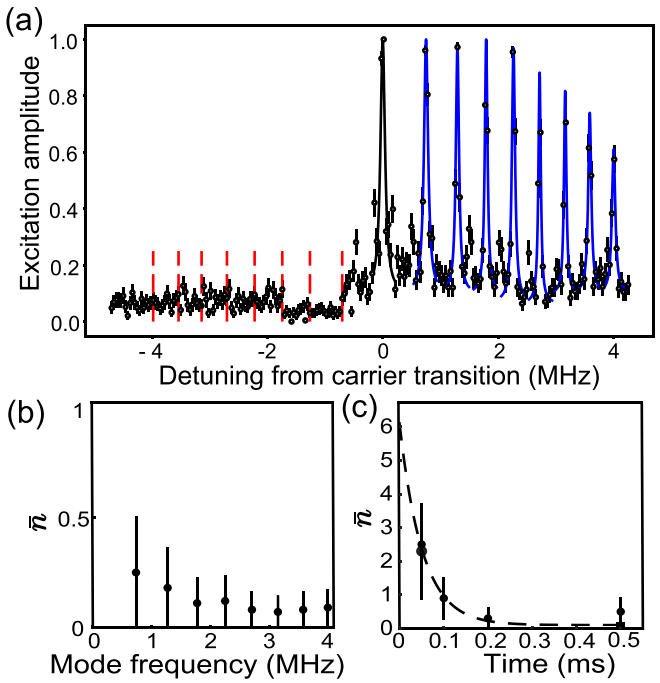

FIG. 3. CRSC of an eight-ion chain. (a) Motional sideband spectrum of an eight-ion chain after CRSC. The black points are experimental data, and solid black and blue lines are Lorentzian fits for the carrier and BSB transitions. Dashed vertical red lines mark the calculated RSB transition frequencies. (b) Extracted mean phonon numbers of the motional modes from the re-scaled fittings of the red-to-blue sideband ratios (see text). (c) Cooling dynamics of the c.m. mode in an eight-ion chain. Black points are the extracted $\bar{n}$, and the red line is an exponential fit.

frequency mode. Figure 3(a) shows the motional spectrum of eight ions after 5 ms of CRSC with a fixed probe time of 15 μs, which is chosen to excite all modes with different LD parameters with appreciable amplitudes such that the ratio of collective spin excitation between the lowest- and highest-frequency modes is around 2. The excitation amplitude is extracted from the photon counts of the region of interest (ROI) representing the eight ions' positions from the pixel stream on an electron-multiplying charge-coupled device (EMCCD) camera. The photon counts are normalized to zero when all ions are in the dark state, and 1 when the carrier has the strongest excitation. The data show near-zero RSB and strong BSB excitations. For extracting the $\bar{n}$ of each mode, although the sideband ratio method is valid with individual addressing beams [26], it underestimates when the ions are driven with global excitations as in our case [30,32]. We sequentially scan over each BSB and corresponding RSB with a probe time that maximizes the BSB transition excitation amplitude, measure the red-to-blue ratio R_m, and introduce a scaling factor α_m [30,32]. We then numerically search the best-fitted $\bar{n}_m$ of the value $\bar{n}_m = \alpha_m R_m/(1-\alpha_m R_m)$ based on the time evolution of the Hamiltonian of multispin coupled to one phonon mode of interest:

$$\hat{H}_{\rm int}(t) = \sum_i \sigma_+^{(i)} \exp\{i\eta_{i,m}(\hat{a_m} e^{-i\nu_m t} + \hat{a_m}^\dagger e^{i\nu_m t})\} e^{i(-\delta t)} + \text{H.c.} \tag{2}$$

Here, $(\hbar/2)\Omega_0$ is set to 1 for simplicity, which denotes that the Rabi frequency excludes the motion. $\sigma_+^{(i)}$ is the spin-flip operator on ion i, $\eta_{i,m}$ is the LD parameter (of ion i, mode m), ν_m is the frequency of mode m, and δ is the laser detuning. We extract $\bar{n}_m$ for all modes to be below 0.25 [Fig. 3(b)], with errors limited by statistical uncertainties. In addition, we measure the cooling dynamics of the c.m. mode in an eight-ion chain and find the cooling time constant to be 52 μs [Fig. 3(c)]. Given the same total Raman laser power used for cooling, the experiment rate scales faster than numerical simulations [$\mathcal{T} \sim O(\ln n)$], possibly due to additional off-resonant coupling to higher-order modes for multi-ion cases.

V. COOLING A 24-ION CHAIN AT THE OPPOSITE LIMIT OF LDR

Finally, we extend the CRSC technique to the near-opposite limit of LDR: $\eta > 1$ [28]. For small systems such as one or two ions, sideband cooling through the first-order RSB transition becomes inefficient [23], and the dynamics are complicated because of the quasicontinuous energy spectrum from mode mixings [33,49]. We apply 5 ms of CRSC on the second-order RSB to reach $\bar{n} = 0.27(9)$ for a single ion at $\eta = 1.3$, consistent with the recoil limit (see Appendix D). However, with dozens of ions in a long chain, the first-order modes become dominant again due to the large effective mass,

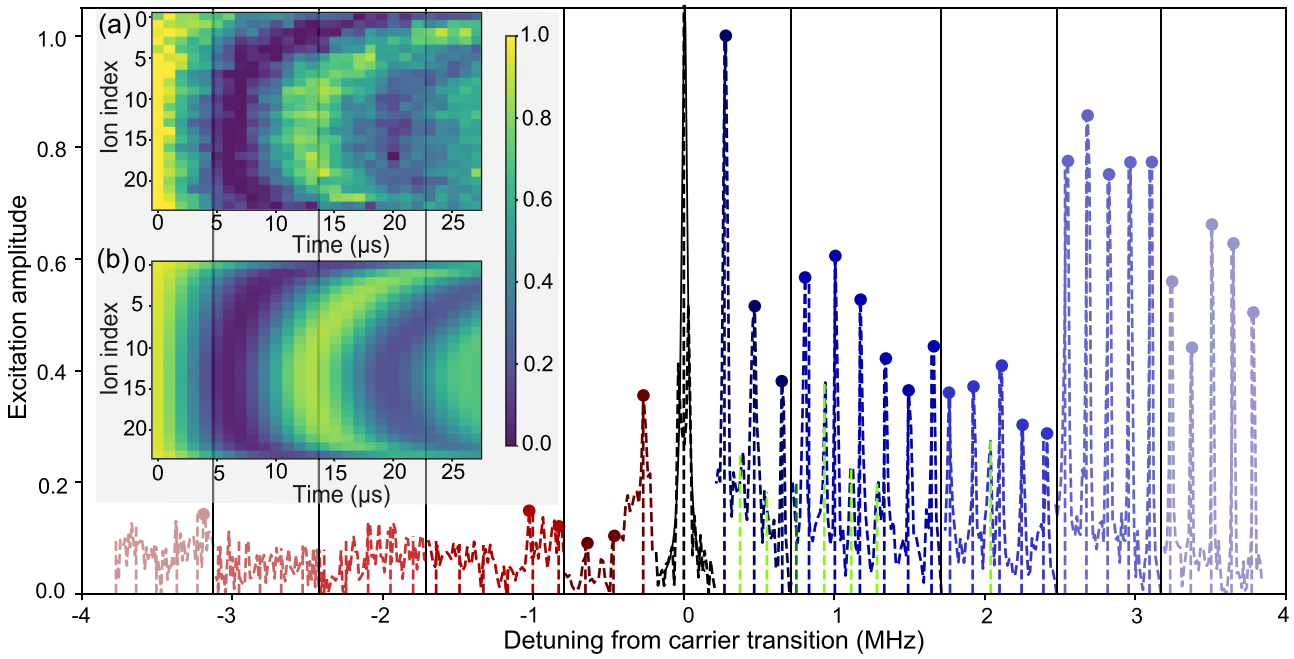

FIG. 4. The frequency spectrum of a 24-ion chain with c.m. mode $\eta = 1.3$ after 10 ms of CRSC. Dashed lines are the experimental results of normalized excitation level versus frequency, where red, black, and blue denote the scan over RSB, carrier, and BSB transitions, respectively. The brightness of the dashed line shows the variable probe times (30, 45, 50, 60, and 70 μs from the darkest to the lightest colors, with solid black lines separating them) throughout the spectrum to ensure that all modes are excited with high visibilities, compensating the large differences of LD parameters between the low- and high-frequency modes. Dashed vertical blue and red lines show all 24 calculated first-order BSB and RSB frequencies. Dashed vertical green lines show the mode mixings between c.m. and a few higher frequency modes, coinciding with the smaller peaks in the experimental data. Inset: (a) Spin dynamics of the carrier Rabi flopping after 10 ms of CRSC. The horizontal axis is the probe time, and the vertical axis is the ion index. (b) Numerical simulation with a c.m. mode $\bar{n} = 1.5$, with experimental Raman beam profiles. Note that the carrier Rabi frequency has a strong modulation across the ion chain due to the different coupling factors $C_i = \prod_{m=1}^{M} e^{-\eta_{i,m}^2/2}$.

reducing the LD factor for each mode. By addressing all the first-order RSBs and applying CRSC for an extended duration of 10 ms, we demonstrate near-ground-state cooling in a 24-ion chain by scanning the sideband spectrum (Fig. 4), with mode LD parameter range (0.33,1.3). The excitation amplitude is extracted using the same method as in the eight-ion case. We observe all 24 first-order BSBs, where the calculated mode frequencies agree well with the experiment. In addition, several small mixing modes between the c.m. mode and higher frequency modes are visible. The RSB transitions are highly suppressed, with near-zero excitations except for the c.m. mode. Owing to spatial correlations of the electrical field noise, the heating rate for the c.m. mode scales with the ion number linearly, with equilibrium $\bar{n}$ balanced between the heating and cooling rates [36]. Since numerically calculating the scaling factors in the sideband ratio method becomes difficult for such a large quantum system [50], we evaluate the cooling effectiveness by analyzing the carrier Rabi flopping. The inset of Fig. 4 shows the experimental result of 24 spin excitations and the numerical simulation of the spin dynamics with a conservatively estimated c.m. mode $\bar{n}$ of 1.5, where all other modes are presumed to have ground-state occupation. The spatial inhomogeneity partially arises from the Gaussian laser beam intensity distribution, which is taken into account in our simulation, but also reflects the spatial dependence in coupling to different modes at such a high LD parameter: the edge ions have ∼16% slower Rabi rates than the center ions even at motional ground states, with laser beams homogeneously illuminating the chain. Our result puts a lower bound on the power of the CRSC technique, where the speed could be further improved by optimizing the power distribution of cooling each mode (see Appendix B), using numerical methods such as machine learning [51], and the temperature could be lowered by other subrecoil techniques such as velocity-selective coherent population trapping [52].

VI. CONCLUSION

In summary, we demonstrate a continuous Raman sideband cooling scheme scalable for large trapped ion systems on account of its flexibility, robustness, efficiency, and high bandwidth. These advantages over the traditional schemes are extended far outside the Lamb-Dicke regime. Our method can be readily generalized to three-dimensional ground-state cooling [17], mixed-species ion systems [6,53], sympathetic cooling of molecular [29,54] and highly charged ions [55], and high-dimensional Coulomb crystals [32,33,36]. It also applies to many other systems such as atoms or molecules in optical tweezer arrays [22,23] and optical lattices [20,21]. Our study presents a crucial step towards large-scale quantum simulation [4] and computation [27] beyond dozens of qubits.

ACKNOWLEDGMENTS

We thank Ye Wang, Wenchao Ge, Yong Wan, and Zijian Ding for helpful discussions and critical reading of the manuscript.

APPENDIX A: SINGLE-ION COOLING SPEED ANALYSIS

In this section, we provide a numerical simulation of cooling speed at various optical pumping powers and compare the cooling rate of CRSC with pulsed Raman sideband cooling (PRSC).

1. Cooling speed versus optical pumping power

To understand the optimal parameters for continuous Raman sideband cooling, we conduct numerical studies and compare them with the experiment. The optical pumping power is critical to the cooling speed and final temperature: it needs to be tuned to a moderate power depending on the carrier Rabi frequency so that the populations quickly reach steady-state values. For a single ion, we consider the four relevant atomic levels involved in CRSC to model the cooling dynamics [as shown in Fig. 5(a): $|1\rangle \equiv |\downarrow\rangle$, $|2\rangle \equiv |\uparrow\rangle$, $|3\rangle \equiv |\text{aux}\rangle$ and $|4\rangle \equiv |e\rangle$]. Under the RSB Raman drive Ω_{12} and two optical pumpings Ω_{24} and Ω_{34}, the Hamiltonian has the form of

$$\mathcal{H} = \begin{pmatrix} 0 & \frac{\Omega_{12}}{2} & 0 & 0 \\ \frac{\Omega_{12}}{2} & 0 & 0 & \frac{\Omega_{24}}{2} \\ 0 & 0 & -\delta & \frac{\Omega_{34}}{2} \\ 0 & \frac{\Omega_{24}}{2} & \frac{\Omega_{34}}{2} & 0 \end{pmatrix}. \tag{A1}$$

Assuming the motion is in a thermal state during the cooling process, Ω_{12} is the average Rabi frequency of the RSB transition between different number states:

$$\Omega_{12}(\bar{n}) = \Omega_0 \sum_{n=1}^{\infty} \frac{\bar{n}^n}{(\bar{n}+1)^{n+1}} e^{-\eta^2/2} \eta \frac{1}{\sqrt{n}} L_n^{(1)}(\eta^2), \tag{A2}$$

where $\bar{n}$ is the mean phonon number, η is the LD parameter, and $L_n^{(1)}(\eta^2)$ are the generalized Laguerre polynomials. During our experiment, $\Omega_0/2\pi = 300$ kHz is the Rabi frequency of the atomic transition. The pumping speed is set to Ω_R with the Rabi frequencies of the two pumping beams $R_1 : \Omega_{24}/2\pi = 700$ kHz and $R_2 : \Omega_{34}/2\pi = 600$ kHz (R_2). $\delta/2\pi = 10$ kHz is the detuning of the R_2 beam from atomic resonance to avoid coherent population trapping. To include spontaneous emission from the $|4\rangle$ state, the system evolution can be described by Lindblad equation:

$$\frac{d\rho}{dt} = \frac{1}{i\hbar}[\mathcal{H}, \rho] + \mathcal{K}\rho, \tag{A3}$$

where ρ is the density matrix of the four-level system, and $\mathcal{K}\rho = -\frac{1}{2}\sum_{m=1}^{3}[\hat{C}_m^\dagger \hat{C}_m \rho + \rho \hat{C}_m^\dagger \hat{C}_m + \hat{C}_m \rho \hat{C}_m^\dagger]$ denotes the dissipation through the three decay channels $\hat{C}_1 = \sqrt{\Gamma \times 2/3}\,|1\rangle\langle 4|$, $\hat{C}_2 = \sqrt{\Gamma/4}\,|2\rangle\langle 4|$, and $\hat{C}_3 = \sqrt{\Gamma/12}\,|3\rangle\langle 4|$. Γ is the natural linewidth of the $^2P_{3/2}$ state of $^9Be^+$. The cooling rate approximately equals the number of photons scattering from state $|4\rangle$ to state $|1\rangle$:

$$\frac{d\bar{n}}{dt} \approx -\frac{\Gamma_{41}}{3}\rho_{44}(t). \tag{A4}$$

We extract the time evolution of $\bar{n}$ from the numerical solutions of Eqs. (A3) and (A4). To show the influence of optical pumping on the cooling effect, in Fig. 5(b), we compare the single-ion cooling dynamics with different optical pumping speeds: $0.2\Omega_R$, $0.4\Omega_R$, Ω_R, $2.5\Omega_R$ and $5\Omega_R$, with Ω_R being

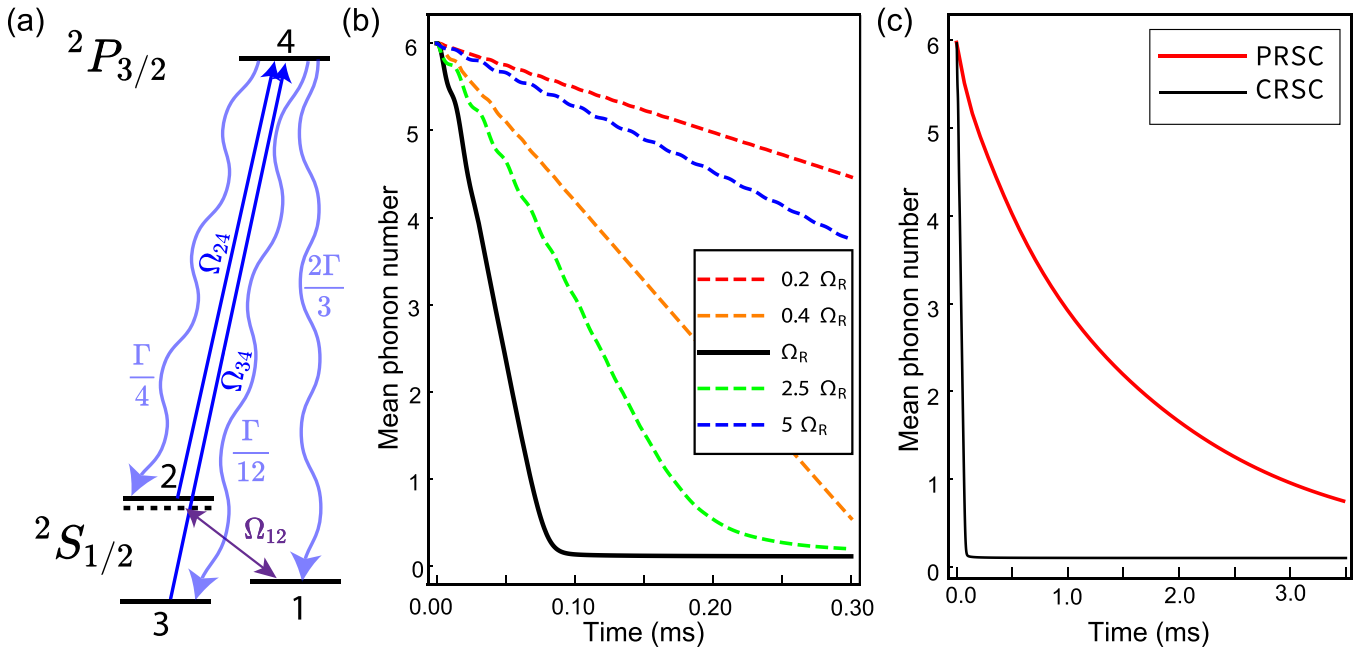

FIG. 5. (a) Illustration of the four-level system for the numerical study of CRSC with the master equation method. (b) Numerical simulation of CRSC dynamics in 300 μs of a single ion under different optical pumping Rabi frequencies. (c) Comparison of CRSC dynamics with optimal pumping power and PRSC with optimal pulse length.

the optimal value: cooling to near the ground state takes about 200 μs, which agrees with the experiment.

2. Cooling speed: Continuous versus pulsed

To show the cooling efficiency of our scheme compared to the more traditional pulsed sideband cooling, we numerically simulate the cooling speeds of CRSC and PRSC of a single ion. We model the PRSC process with the same carrier Rabi frequency of $\Omega_0/2\pi = 300$ kHz, LD parameter $\eta = 0.78$, and initial thermal phonon state $\bar{n} = 6$. For simplicity, we ignore the optical pumping time and photon-recoil effects and set each pulse to equal length t, which shows close to optimal cooling times. The phonon population after the ith pulse can be written as a function of the population after the previous pulse:

$$\begin{aligned}
P_i(0) &= P_{i-1}(0) + \tfrac{1}{2}P_{i-1}(1)(1-\cos\Omega_{0,1}t),\\
P_i(1) &= \tfrac{1}{2}P_{i-1}(1)(1+\cos\Omega_{0,1}t) + \tfrac{1}{2}P_{i-1}(2)(1-\cos\Omega_{1,2}t),\\
&\vdots\\
P_i(n) &= \tfrac{1}{2}P_{i-1}(n)(1+\cos\Omega_{n-1,n}t) + \tfrac{1}{2}P_{i-1}(n+1)\\
&\quad\times(1-\cos\Omega_{n,n+1}t),
\end{aligned} \tag{A5}$$

where $P_i(n)$ denotes the population on the $|n\rangle$ state in the i step, and $\Omega_{n,n+1}$ is the Rabi frequency of the $|\uparrow, n+1\rangle \leftrightarrow |\downarrow, n\rangle$ transition. We numerically search the optimal pulse length between 0 and 100 μs that yields the lowest $\bar{n}$ after 50 cooling pulses and find $T = 71.5$ μs. Figure 5(c) shows the cooling time comparisons, in which PRSC is significantly slower, and the $\bar{n}$ does not reach the ground state after 3.5 ms. An intuitive reason for the speedup is the following: in the CRSC process, the state population will quickly reach a steady state under an appropriate optical pumping rate. This guarantees the fastest pumping rate towards the motional ground state. whereas in the PRSC, the instant population transfer rate towards the ground state varies between zero and maximum and can be negative when the pulse is overdriven. CRSC is also more robust than PRSC: it avoids complicated optimization of cooling pulses, driving higher-order sidebands when the ions are outside the LDR, and is not sensitive to timing error.

APPENDIX B: COOLING SPEED SCALING WITH ION NUMBER

Beyond a single ion, we analyze the cooling of multiple modes in a long ion chain and compare the cooling efficiency of our parallel approach to the traditional sequential scheme, assuming the fixed optical power. The cooling time to the ground state of a single ion is $\mathcal{T}_1 = A\bar{n}_1/(\eta\Omega_0) = 200$ μs, where A is a constant and $\bar{n}_1$ is the initial mean phonon number. Generalizing to an N-ion chain, we assume all modes are resolved in frequency, and each mode is cooled to the Doppler limit. The cooling time for mode m is $\mathcal{T}_m = A\bar{n}_m/(\eta_m\Omega_m)$, where $\bar{n}_m \propto 1/\omega_m$ is the initial mean phonon number of the mode, $\eta_m \propto 1/\sqrt{\omega_m}$ is the mode LD parameter, and $\Omega_m \propto \sqrt{P_m}$ is the Rabi frequency component on the mode. The total cooling time can be written as

$$\mathcal{T} = \max_m\left(\frac{C}{\sqrt{\omega_1 P_1}}, \frac{C}{\sqrt{\omega_2 P_2}}, \ldots, \frac{C}{\sqrt{\omega_N P_N}}\right), \tag{B1}$$

with $\sum_m P_m = P_0$. The total cooling time is the shortest $\mathcal{T}_{min}$ when $\omega_1 P_1 = \omega_2 P_2 = \cdots = \omega_N P_N$. So we have $\mathcal{T}_{min}$ cooling

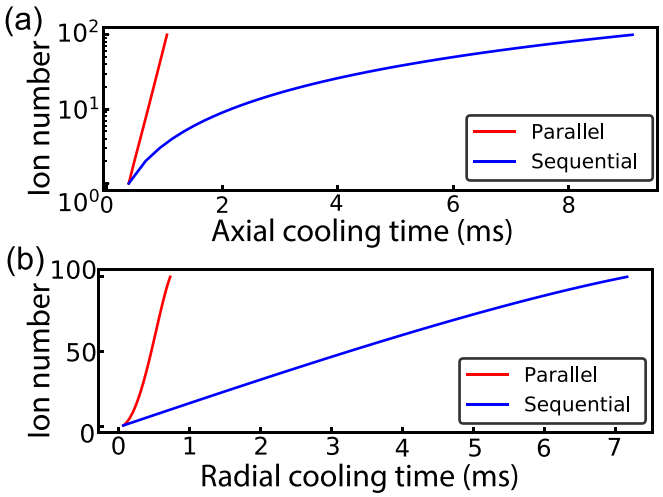

FIG. 6. Numerical simulation of (a) axial and (b) radial modes cooling time scaling with the increase of ion number, comparing our parallel with the traditional sequential scheme.

axial modes of an N-ion chain:

$$\mathcal{T}_{min}^{N} = \sqrt{\omega_1 \sum_{m=1}^{N} \frac{1}{\omega_m}} \mathcal{T}_1 \sim O(\ln N)\mathcal{T}_1, \tag{B2}$$

for which the cooling speed scaling of 8 ions compared to a single ion agrees with the experiment. In the traditional scheme, the total cooling time $\mathcal{T}_{min}^{\prime N}$ equals the sum of the time spent in cooling each mode:

$$\mathcal{T}_{min}^{\prime N} = \sqrt{\omega_1} \sum_{m=1}^{N} \frac{1}{\sqrt{\omega_m}} \mathcal{T}_1 \sim O(N)\mathcal{T}_1. \tag{B3}$$

Compared to traditional sequential cooling, our scheme provides an exponential speedup for axial modes in the ion number scaling, which is especially powerful when cooling large ion crystals. To illustrate this, we compare the cooling time with the increase of ion number of parallel versus sequential cooling in our numerics. We assume single-ion motional frequency $(\omega_x, \omega_z)/2\pi = (7.5, 0.2)$ MHz to maintain a linear chain when trapping many ions. Based on Eqs. (B2) and (B3), in Figs. 6(a) and 6(b) we calculate the cooling time scaling of axial and radial modes, respectively, up to 100 ions. While our scheme for cooling the axial modes has exponential speedup, cooling for the radial modes scales as $O(N)$, similar to the traditional method. However, the total cooling time is less than 1 ms which makes the scheme scalable. Furthermore, we expect the cooling time to be independent of ion number if all modes are not resolvable. Another advantage is that our scheme is more convenient for balancing the cooling and heating mechanisms. Cooling a specific motional mode introduces heating for other modes due to recoil heating from scattering photons. However, in our parallel scheme, both the cooling and recoil heating rate are proportional to $1/\omega_m$, which would facilitate cooling towards the ground state for all modes simultaneously.

APPENDIX C: MEASUREMENT OF MULTI-ION PHONON NUMBERS

In this section, we discuss two methods to assess the cooling effects of CRSC.

1. Multi-ion phonon number extraction from sideband ratio

Following the discussion in the main text, the traditional sideband ratio method underestimates the phonon number for the multi-ion case. For example, in a two-ion crystal at the $n = 1$ state of its c.m. mode, the BSB flopping will involve $n = 1$, $n = 1$, and $n = 3$ states, while the RSB flopping will only involve $n = 0$ and $n = 1$. The asymmetry nullifies the sideband ratio method, and the Jaynes-Cummings model no longer captures the dynamics. Therefore, we introduce a scaling factor α to compensate for the underestimation. To further understand the multispin phonon dynamics, we numerically study the time evolution of RSB and BSB transitions on each mode, for which the Hamiltonian can be described as

$$H_{rsb,m} = (\hbar/2)\Omega_0 \sum_{i=1}^{N} \sigma_+^{(i)} \left(\eta_{i,m} a_m + \eta_{i,m}^3 a_m^2 a_m^\dagger/2\right) + \text{H.c.},$$
$$H_{bsb,m} = (\hbar/2)\Omega_0 \sum_{i=1}^{N} \sigma_+^{(i)} \left(\eta_{i,m} a_m^\dagger + \eta_{i,m}^3 a_m^{\dagger 2} a_m/2\right) + \text{H.c.} \tag{C1}$$

Here, the Pauli operator $\sigma_+^{(i)} = 1/2(\sigma_x^{(i)} + i\sigma_y^{(i)})$ acts on the ith ion, a_m and $a_m^\dagger$ are the creation and annihilation operators on the mth mode, and $\eta_{i,m}$ is the Lamb-Dicke parameter of the ith ion and mth mode. Here we keep the Lamb-Dicke expansion to the third order. We assume the phonons are thermally populated with mean phonon number $\overline{n_m}$. Then we apply a numerical simulation of the time evolution under the RSB and BSB drive with the initial state:

$$|i\rangle_{\overline{n_m}} = |\uparrow\uparrow\cdots\uparrow\rangle \otimes \sum_{n_m} \frac{\overline{n_m}^{n_m}}{(\overline{n_m}+1)^{n_m+1}} |n_m\rangle\langle n_m|. \tag{C2}$$

The result states $|r\rangle_{\overline{n_m}}(t)$ and $|b\rangle_{\overline{n_m}}(t)$ have brightnesses of $A_{\overline{n_m},r}(t)$ and $A_{\overline{n_m},b}(t)$. After T, the BSB flops to the brightest state, and we can calculate the RSB to BSB amplitude:

$$R(\overline{n_m}) = A_{\overline{n_m},r}(T)/A_{\overline{n_m},b}(T), \tag{C3}$$

which is a function of the mode index m and the corresponding mean phonon number. In the case of a single ion $R = \overline{n}/(\overline{n}+1)$. We experimentally measure the RSB to BSB amplitude when BSB is the brightest $R_{m,expt}$ and extract $\overline{n_m}$ from the inverse function of $R(\overline{n_m})$. In other words, we introduce a scaling factor α_m so that the mean phonon number of the mode can be calculated as $\bar{n}_m = \alpha_m R_m/(1-\alpha_m R_m)$. α_m is mode specific and phonon sensitive ($\alpha = 1$ for the single-ion case). In Fig. 7 we show the experimental data of BSB and BSB spectra. The BSB peaks are normalized to 1 for the excitation amplitude of each mode. RSB peaks are not visible, and we use half of the peak-to-peak noise to give an upper bound of the RSB excitation amplitude $A_{\overline{n_m},r}(T)$. From the frequency spectra, we extract $\bar{n} = \{0.25(24), 0.18(18), 0.11(11), 0.12(11), 0.09(9), 0.07(7), 0.08(8), 0.09(8)\}$ from the lowest- to highest-order modes of an eight-ion chain.

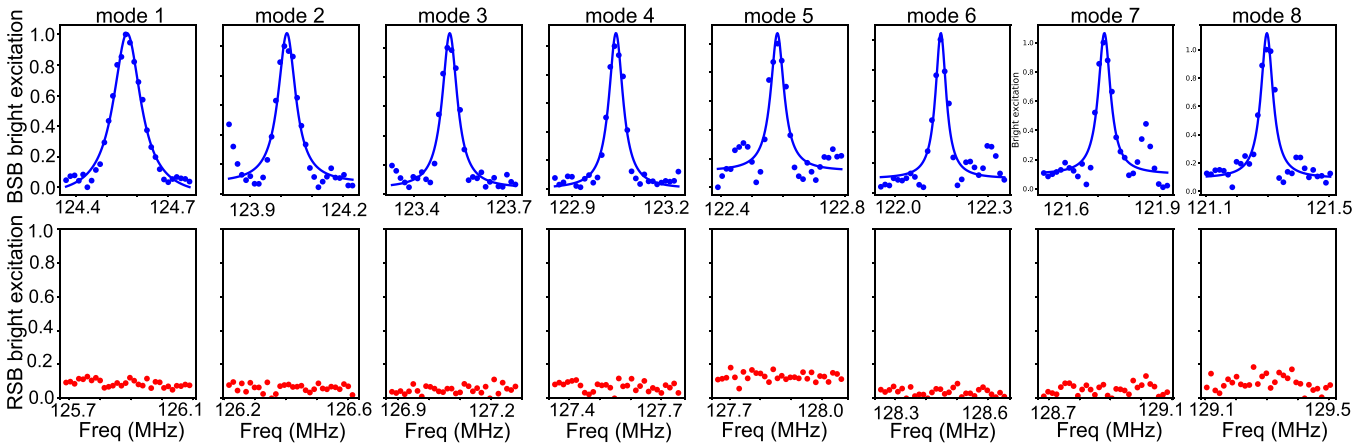

FIG. 7. Frequency scan of eight-ion chain on BSB and RSB transitions. Blue and red points are the experimental data for BSB and RSB transitions, respectively. Solid blue lines are Gaussian fits to the BSB data.

Although this method has large uncertainty compared to the single-ion case, it puts an upper bound on the final temperature without using individual addressing beams.

2. Multi-ion carrier flopping

Besides scanning the frequency spectrum, analyzing the carrier Rabi flopping is an alternative method to evaluate the cooling effect. Multi-ion carrier flopping under thermal motion can be complicated as ions can be modulated by phonons from all the modes. Now we consider the ion i carrier transition, which couples to all the M modes. In the LD regime a good approximation of the Rabi frequency is $\bar{\Omega}_i = \Omega_i \exp[-\sum_m \eta_{im}^2(\bar{n}_m + 1/2)]$. And one can evaluate the cooling effect from the contrast of carrier flopping. However, extracting the mean phonon number from a certain mode is hard. And the dynamics become nontrivial when ions are far outside the LD regime as in our case. The carrier Hamiltonian can be written as

$$H_{i,M} = (\hbar/2)\Omega_i \sigma_+^{(i)} \prod_{m=1}^{M} \exp[i\eta_{i,m}[a_m + a_m^+)] + \text{ H.c.} \quad \text{(C4)}$$

For a specific number state $n_1, n_2, \ldots, n_M$, the carrier Rabi frequency is

$$\begin{aligned}\Omega^{(i)} &= (\hbar/2)\Omega_0^{(i)} \langle n_1, n_2, \ldots, n_M| \\ &\quad \times \prod_{m=1}^{M} \exp[i\eta_{i,m}[a_m + a_m^+)]|n_1, n_2, \ldots, n_M\rangle \\ &= \prod_{m=1}^{M} e^{-\eta_{i,m}^2/2} \mathrm{L}_{n_m}\left(\eta_{i,m}^2\right)\Omega_0^{(i)}. \end{aligned} \quad \text{(C5)}$$

If the ions are cooled to the ground state, the carrier Rabi frequency equals $\prod_{m=1}^{M} e^{-\eta_{i,m}^2/2}\Omega_0^{(i)}$. Note that in the axial c.m. mode $\eta = 1.3$ of a 24 Be^+ chain, the center ions have 19% stronger Rabi frequency than the edge ions. If we cut off the phonon state to $n = 9$, for 24 ions with 24 modes, we need to consider in total 10^{24} transitions, each one corresponding to frequency $\Omega_{n,n}$ and a phonon state population of

$$P_n = \prod_{m=1}^{M} \frac{\overline{n_m}^n}{(\overline{n_m} + 1)^{n+1}}. \quad \text{(C6)}$$

So the time evolution of the carrier Rabi flopping is

$$P_i(t) = \frac{1}{2}\left(1 + \sum_m (P_n \cos(\Omega_{n,n} t)\right), \quad \text{(C7)}$$

where $P_i(t)$ is the population on $|\downarrow\rangle$ at time t. From the previous method, since virtually no RSB excitation except the c.m. mode appears on the 24-ion spectrum, we simplify the model by considering only thermal distribution on the c.m. mode (discussed in the main text) and assume all other modes are cooled to the ground state. In Fig. 8 the black points show the carrier time flop of individual ions. We perform an exponential fit to all the ions, as shown by the solid blue lines, then numerically search the best-fitted c.m. mode $\bar{n}$ to the exponential fits (orange lines).

APPENDIX D: COOLING LIMIT DISCUSSION

In this section, we discuss several factors which could limit the final cooling temperature.

1. Electric field noise-induced heating

We measure the cooling and heating rate of a single ion's axial motion under the trap frequency $\omega_1/2\pi = 735$ kHz ($\eta = 0.78$) to be $R_c^0 = 3.2 \times 10^4$/s and $R_h^0 = 2.0 \times 10^2$/s, respectively. The cooling speed R_c scales as $1/\ln N$, limited by the laser intensity in each cooling tone and is proportional to the Lamb-Dicke parameter η. On the other hand, heating of the c.m. mode scales as N and is proportional to $\omega^{-(\alpha+1)}$. α gauges the noise intensity at a certain frequency. Based on the previous experiments on heating rate measurements without surface treatments [56], we can conservatively assume $\alpha = 1$, which considers the $1/f$ noise. We estimate the cooling and heating rate of the c.m. mode of a 24-ion chain under the axial

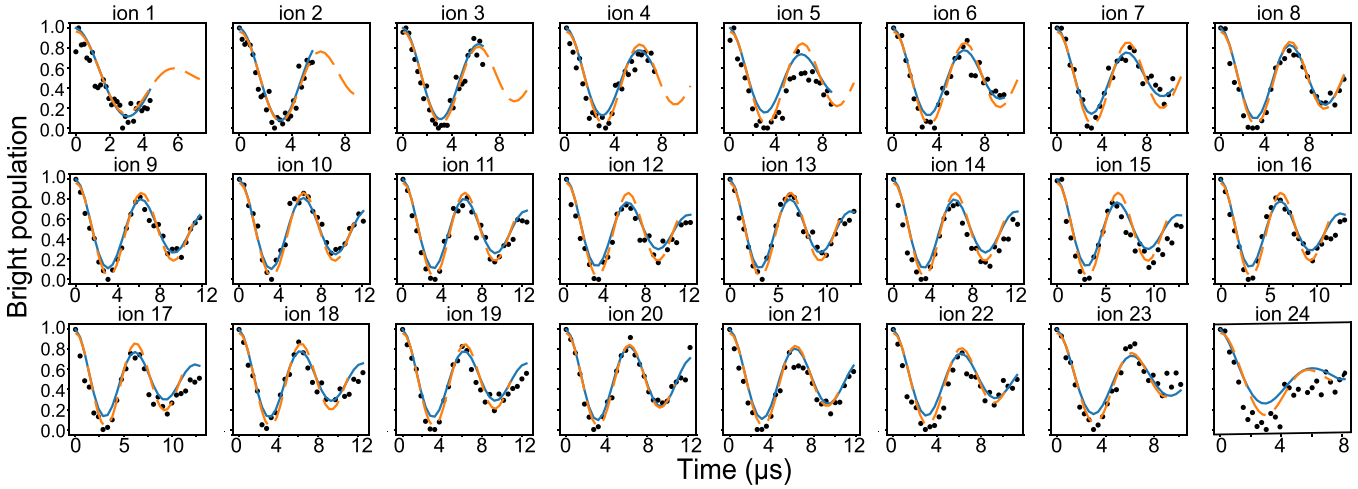

FIG. 8. Normalized excitation amplitude of a 24-ion chain on an EMCCD camera. Black points are the experimental data, solid blue lines are the experimental fit, and dashed orange lines are the numerical simulation of the fitted c.m. mode $\bar{n} = 1.5$.

frequency of $\omega_2/2\pi = 272$ kHz:

$$R_c^N = R_c^0\sqrt{\omega_1/\omega_2}/\ln(N) = 1.6 \times 10^4/\text{s},$$
$$R_h^N = NR_h^0(\omega_1/\omega_2)^2 = 3.5 \times 10^4/\text{s}. \quad \text{(D1)}$$

So the equilibrium $\bar{n} = R_h^N/R_c^N = 2.2$, which agrees with the extraction we get from carrier flopping $\bar{n} = 1.5$.

2. Photon recoil heating

Figure 9 shows carrier flopping of a single ion at $\eta = 1.3$ after 5 ms of CRSC on the second-order RSB; the measured $\bar{n} = 0.27(9)$ is most likely limited by photon-recoil effects. We first consider the fundamental cooling limit of photon recoils during CRSC. When the Raman beam drives the qubit on the first-order RSB of $|\downarrow\rangle \leftrightarrow |\downarrow\rangle$ and removes a phonon, optical pumping is required to initiate the qubit in the $|\downarrow\rangle$ state, which absorbs and emits 1.5 photons on average. So the heating from spin-reset optical pumping is

$$\Delta n_h = (\Delta E_{\text{ab}} + \Delta E_{\text{em}})/\hbar\omega_z$$
$$\simeq 1.5\left(\tfrac{1}{2} + \tfrac{1}{3}\right)\tilde{\eta}^2$$
$$= 1.25\tilde{\eta}^2, \quad \text{(D2)}$$

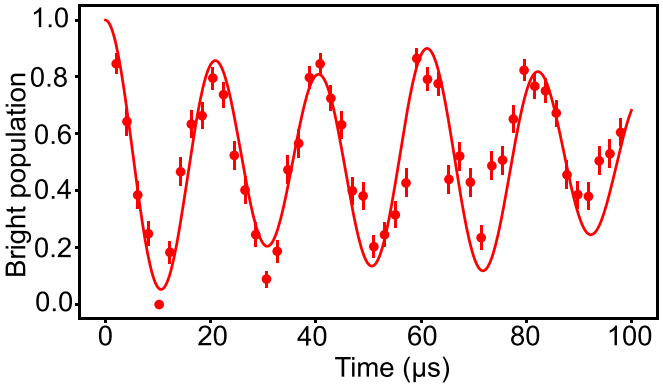

FIG. 9. Carrier flopping of a single ion at $\eta = 1.3$ after CRSC. Red points are the measurement data, and the solid red line is a least-squares fit to the measurements with $\bar{n} = 0.27(9)$.

where ΔE_{abs} and ΔE_{em} are the single-photon recoil energy of absorption and emission into the axial direction; 1/2 and 1/3 come from the energy components of the absorbed and emitted photon in the axial direction. $\tilde{\eta} = \eta/\sqrt{2}$ is the single-photon Lamb-Dicke parameter. So the recoil heatings at the two LD parameters used in the experiment are $\Delta n_h^{(1)} = 0.38$ ($\eta = 0.78$) and $\Delta n_h^{(2)} = 1.1$ ($\eta = 1.3$). This justifies that at $\eta = 0.78$ ground-state cooling can be done by driving the first-order RSB ($\Delta n_h^{(1)} < 1$), while at $\eta = 1.3$ we must couple to the higher-order RSB ($\Delta n_h^{(2)} > 1$). In principle, sideband cooling is not recoil limited. However, there are several technical limiting factors which generate additional recoil heatings:

(1) At the end of CRSC, we apply 2 μs optical pumping at $s = 0.8$ ($s = I/I_{sat}$) to clean up the population on $|\uparrow\rangle$ and $|\text{aux}\rangle$ states. One of the pumping beams is 120 MHz red detuned from the qubit Doppler transition. This step scatters 0.5 photons on average and heats up the ions: $\Delta n_h^{(1)} = 0.13$ ($\eta = 0.78$) and $\Delta n_h^{(2)} = 0.35$ ($\eta = 1.3$).

(2) During the CRSC, the 120 MHz red-detuned pumping beam off-resonantly couples to Doppler transition ($s = 0.4$), corresponding to a 125-kHz photon scattering rate. This part of heating rates on the ions gives $\dot{n}_{h1}^{(1)} = 31$ kHz ($\eta = 0.78$) and $\dot{n}_{h1}^{(2)} = 86$ kHz ($\eta = 1.3$).

(3) Off-resonant coupling to the carrier transition. The transition rate is $\Omega_{off} = \Omega_c^3/(\Omega_c^2 + \Delta^2)$, and the photon scattering rate is equal to $1.5\Omega_{off}/(2\pi)$. This part of heating on the ions gives $\dot{n}_{h2}^{(1)} = 3.0$ kHz ($\eta = 0.78$) and $\dot{n}_{h2}^{(2)} = 7.8$ kHz ($\eta = 1.3$).

In summary, extra recoil heating is the limiting factor for the final temperature. Adding a few cycles of microwave-assisted pumping [29] with Rabi π pulse from the $|\text{aux}\rangle$ state to the $|\uparrow\rangle$ state followed by the weak pumping beam to clear out $|\uparrow\rangle$ will highly suppress the off-resonant recoils.

3. Background gas collisions

Finally, we consider the heating caused by background gas collisions. As our vacuum is mainly limited by the existence of molecular hydrogen gas that is orders of magnitude

more than other species, we assume that all collisions are induced by hydrogen. With room-temperature (300 K) hydrogen molecules colliding with the beryllium ions under the hard-sphere collision model, we find a mean energy of $E_{\mathrm{BGC}} = 6.2 \times 10^{-22}$ J [57]. We further assume that E_{BGC} fills in equally to all M modes. As $M = 3N$, for a single collision event, we have a mean energy of

$$\omega_{\mathrm{BGC}}/2\pi = \frac{E_{\mathrm{BGC}}}{3N \times 2\pi\hbar} = 1.30 \times 10^{10}\ \mathrm{Hz}. \tag{D3}$$

This leads to $\bar{n} = 47000$, which is far beyond the Doppler cooling limit. Such collisions usually lead to the melting of the entire chain when the Doppler cooling light is off, and it is observable: hydrogen molecules collision "melt" the ion chain, and the ions go into a "cloud state" with much weaker fluorescence. Therefore, the heating of background gas collisions is avoided by discarding the affected outliers, which are easily distinguishable and only account for a small portion of the total data.

We measure the collision rate R_{BGC} in our vacuum system by counting the number of ion-ion hopping events per second. We find that on average $R_{\mathrm{BGC}} = 0.07$ event/(ion s), which is consistent with our estimation based on the vacuum pressure. So with 24 ions in the chain, we expect 0.168 collisions per second. Furthermore, as the time for a single run of an experiment is on the scale of 1 ms, we can assume a second is equivalent to 100 experiments. So we expect 1.6×10^{-3} collision per experiment, making the melting data account for 0.2% of the total data.

[1] S. Debnath, N. M. Linke, C. Figgatt, K. A. Landsman, K. Wright, and C. Monroe, Demonstration of a small programmable quantum computer with atomic qubits, Nature (London) **536**, 63 (2016).

[2] I. Pogorelov, T. Feldker, C. D. Marciniak, L. Postler, G. Jacob, O. Krieglsteiner, V. Podlesnic, M. Meth, V. Negnevitsky, M. Stadler *et al.*, Compact ion-trap quantum computing demonstrator, PRX Quantum **2**, 020343 (2021).

[3] T. Manovitz, Y. Shapira, L. Gazit, N. Akerman, and R. Ozeri, Trapped-ion quantum computer with robust entangling gates and quantum coherent feedback, PRX Quantum **3**, 010347 (2022).

[4] J. Zhang, G. Pagano, P. W. Hess, A. Kyprianidis, P. Becker, H. Kaplan, A. V. Gorshkov, Z.-X. Gong, and C. Monroe, Observation of a many-body dynamical phase transition with a 53-qubit quantum simulator, Nature (London) **551**, 601 (2017).

[5] P. Jurcevic, B. P. Lanyon, P. Hauke, C. Hempel, P. Zoller, R. Blatt, and C. F. Roos, Quasiparticle engineering and entanglement propagation in a quantum many-body system, Nature (London) **511**, 202 (2014).

[6] J.-S. Chen, S. M. Brewer, C. W. Chou, D. J. Wineland, D. R. Leibrandt, and D. B. Hume, Sympathetic Ground State Cooling and Time-Dilation Shifts in an $^{27}Al^{+}$ Optical Clock, Phys. Rev. Lett. **118**, 053002 (2017).

[7] C. Sanner, N. Huntemann, R. Lange, C. Tamm, E. Peik, M. S. Safronova, and S. G. Porsev, Optical clock comparison for Lorentz symmetry testing, Nature (London) **567**, 204 (2019).

[8] P. Micke, T. Leopold, S. King, E. Benkler, L. Spieß, L. Schmoeger, M. Schwarz, J. Crespo López-Urrutia, and P. Schmidt, Coherent laser spectroscopy of highly charged ions using quantum logic, Nature (London) **578**, 60 (2020).

[9] T. P. Harty, D. T. C. Allcock, C. J. Ballance, L. Guidoni, H. A. Janacek, N. M. Linke, D. N. Stacey, and D. M. Lucas, High-Fidelity Preparation, Gates, Memory, and Readout of a Trapped-Ion Quantum Bit, Phys. Rev. Lett. **113**, 220501 (2014).

[10] P. Wang, C.-Y. Luan, M. Qiao, M. Um, J. Zhang, Y. Wang, X. Yuan, M. Gu, J. Zhang, and K. Kim, Single ion qubit with estimated coherence time exceeding one hour, Nat. Commun. **12**, 233 (2021).

[11] J. P. Gaebler, T. R. Tan, Y. Lin, Y. Wan, R. Bowler, A. C. Keith, S. Glancy, K. Coakley, E. Knill, D. Leibfried *et al.*, High-Fidelity Universal Gate Set for $^{9}Be^{+}$ Ion Qubits, Phys. Rev. Lett. **117**, 060505 (2016).

[12] C. J. Ballance, T. P. Harty, N. M. Linke, M. A. Sepiol, and D. M. Lucas, High-Fidelity Quantum Logic Gates Using Trapped-Ion Hyperfine Qubits, Phys. Rev. Lett. **117**, 060504 (2016).

[13] C. R. Clark, H. N. Tinkey, B. C. Sawyer, A. M. Meier, K. A. Burkhardt, C. M. Seck, C. M. Shappert, N. D. Guise, C. E. Volin, S. D. Fallek *et al.*, High-Fidelity Bell-State Preparation with $^{40}Ca^{+}$ Optical Qubits, Phys. Rev. Lett. **127**, 130505 (2021).

[14] D. Porras and J. I. Cirac, Effective Quantum Spin Systems with Trapped Ions, Phys. Rev. Lett. **92**, 207901 (2004).

[15] A. Friedenauer, H. Schmitz, J. T. Glueckert, D. Porras, and T. Schätz, Simulating a quantum magnet with trapped ions, Nat. Phys. **4**, 757 (2008).

[16] K. Kim, M.-S. Chang, S. Korenblit, R. Islam, E. E. Edwards, J. K. Freericks, G.-D. Lin, L.-M. Duan, and C. Monroe, Quantum simulation of frustrated Ising spins with trapped ions, Nature (London) **465**, 590 (2010).

[17] C. Monroe, D. M. Meekhof, B. E. King, S. R. Jefferts, W. M. Itano, D. J. Wineland, and P. Gould, Resolved-Sideband Raman Cooling of a Bound Atom to the 3D Zero-Point Energy, Phys. Rev. Lett. **75**, 4011 (1995).

[18] S. E. Hamann, D. L. Haycock, G. Klose, P. H. Pax, I. H. Deutsch, and P. S. Jessen, Resolved-Sideband Raman Cooling to the Ground State of an Optical Lattice, Phys. Rev. Lett. **80**, 4149 (1998).

[19] J. Chan, T. Alegre, A. H. Safavi-Naeini, J. T. Hill, A. Krause, S. Gröblacher, M. Aspelmeyer, and O. Painter, Laser cooling of a nanomechanical oscillator into its quantum ground state, Nature (London) **478**, 89 (2011).

[20] V. Vuletić, C. Chin, A. J. Kerman, and S. Chu, Degenerate Raman Sideband Cooling of Trapped Cesium Atoms at Very High Atomic Densities, Phys. Rev. Lett. **81**, 5768 (1998).

[21] D.-J. Han, S. Wolf, S. Oliver, C. McCormick, M. T. DePue, and D. S. Weiss, 3D Raman Sideband Cooling of Cesium Atoms at High Density, Phys. Rev. Lett. **85**, 724 (2000).

[22] A. M. Kaufman, B. J. Lester, and C. A. Regal, Cooling a Single Atom in an Optical Tweezer to Its Quantum Ground State, Phys. Rev. X **2**, 041014 (2012).

[23] Y. Yu, N. R. Hutzler, J. T. Zhang, L. R. Liu, J. D. Hood, T. Rosenband, and K.-K. Ni, Motional-ground-state cooling outside the Lamb-Dicke regime, Phys. Rev. A **97**, 063423 (2018).

[24] D. J. Wineland, C. Monroe, W. M. Itano, D. Leibfried, B. E. King, and D. M. Meekhof, Experimental issues in coherent quantum-state manipulation of trapped atomic ions, J. Res. Natl. Inst. Stand. Technol. **103**, 259 (1998).

[25] A. J. Rasmusson, M. D'Onofrio, Y. Xie, J. Cui, and P. Richerme, Optimized pulsed sideband cooling and enhanced thermometry of trapped ions, Phys. Rev. A **104**, 043108 (2021).

[26] J.-S. Chen, K. Wright, N. C. Pisenti, D. Murphy, K. M. Beck, K. Landsman, J. M. Amini, and Y. Nam, Efficient-sideband-cooling protocol for long trapped-ion chains, Phys. Rev. A **102**, 043110 (2020).

[27] M. Cetina, L. N. Egan, C. Noel, M. L. Goldman, D. Biswas, A. R. Risinger, D. Zhu, and C. Monroe, Control of transverse motion for quantum gates on individually addressed atomic qubits, PRX Quantum **3**, 010334 (2022).

[28] G. Morigi, J. Cirac, M. Lewenstein, and P. Zoller, Ground-state laser cooling beyond the Lamb-Dicke limit, Europhys. Lett. **39**, 13 (1997).

[29] Y. Wan, F. Gebert, F. Wolf, and P. O. Schmidt, Efficient sympathetic motional-ground-state cooling of a molecular ion, Phys. Rev. A **91**, 043425 (2015).

[30] R. Lechner, C. Maier, C. Hempel, P. Jurcevic, B. P. Lanyon, T. Monz, M. Brownnutt, R. Blatt, and C. F. Roos, Electromagnetically-induced-transparency ground-state cooling of long ion strings, Phys. Rev. A **93**, 053401 (2016).

[31] L. Feng, W. L. Tan, A. De, A. Menon, A. Chu, G. Pagano, and C. Monroe, Efficient Ground-State Cooling of Large Trapped-Ion Chains with an Electromagnetically-Induced-Transparency Tripod Scheme, Phys. Rev. Lett. **125**, 053001 (2020).

[32] M. Qiao, Y. Wang, Z. Cai, B. Du, P. Wang, C. Luan, W. Chen, H.-R. Noh, and K. Kim, Double-Electromagnetically-Induced-Transparency Ground-State Cooling of Stationary Two-Dimensional Ion Crystals, Phys. Rev. Lett. **126**, 023604 (2021).

[33] E. Jordan, K. A. Gilmore, A. Shankar, A. Safavi-Naini, J. G. Bohnet, M. J. Holland, and J. J. Bollinger, Near Ground-State Cooling of Two-Dimensional Trapped-Ion Crystals with More than 100 Ions, Phys. Rev. Lett. **122**, 053603 (2019).

[34] J. Zhang, M.-C. Zhang, Y. Xie, C.-W. Wu, B.-Q. Ou, T. Chen, W.-S. Bao, P. Haljan, W. Wu, S. Zhang, and P.-X. Chen, Parallel Electromagnetically Induced Transparency near Ground-State Cooling of a Trapped-Ion Crystal, Phys. Rev. Appl. **18**, 014022 (2022).

[35] S. Ejtemaee and P. C. Haljan, 3D Sisyphus Cooling of Trapped Ions, Phys. Rev. Lett. **119**, 043001 (2017).

[36] M. Joshi, A. Fabre, C. Maier, T. Brydges, D. Kiesenhofer, H. Hainzer, R. Blatt, and C. Roos, Polarization-gradient cooling of 1D and 2D ion Coulomb crystals, New J. Phys. **22**, 103013 (2020).

[37] W. Li, S. Wolf, L. Klein, D. Budker, C. E. Düllmann, and F. Schmidt-Kaler, Robust polarization gradient cooling of trapped ions, New J. Phys. **24**, 043028 (2022).

[38] A. Sørensen and K. Mølmer, Entanglement and quantum computation with ions in thermal motion, Phys. Rev. A **62**, 022311 (2000).

[39] V. Schäfer, C. Ballance, K. Thirumalai, L. Stephenson, T. Ballance, A. Steane, and D. Lucas, Fast quantum logic gates with trapped-ion qubits, Nature (London) **555**, 75 (2018).

[40] J. D. Wong-Campos, S. A. Moses, K. G. Johnson, and C. Monroe, Demonstration of Two-Atom Entanglement with Ultrafast Optical Pulses, Phys. Rev. Lett. **119**, 230501 (2017).

[41] K. C. McCormick, J. Keller, S. C. Burd, D. J. Wineland, A. C. Wilson, and D. Leibfried, Quantum-enhanced sensing of a single-ion mechanical oscillator, Nature (London) **572**, 86 (2019).

[42] O. Katz, M. Cetina, and C. Monroe, *n*-Body Interactions between Trapped Ion Qubits via Spin-Dependent Squeezing, Phys. Rev. Lett. **129**, 063603 (2022).

[43] J. W. Britton, B. C. Sawyer, A. C. Keith, C.-C. J. Wang, J. K. Freericks, H. Uys, M. J. Biercuk, and J. J. Bollinger, Engineered two-dimensional Ising interactions in a trapped-ion quantum simulator with hundreds of spins, Nature (London) **484**, 489 (2012).

[44] C. Roos, T. Zeiger, H. Rohde, H. C. Nägerl, J. Eschner, D. Leibfried, F. Schmidt-Kaler, and R. Blatt, Quantum State Engineering on an Optical Transition and Decoherence in a Paul Trap, Phys. Rev. Lett. **83**, 4713 (1999).

[45] W. M. Itano, D. J. Heinzen, J. J. Bollinger, and D. J. Wineland, Quantum Zeno effect, Phys. Rev. A **41**, 2295 (1990).

[46] Q. Wu, M. Filzinger, Y. Shi, Z. Wang, and J. Zhang, Adaptively controlled fast production of defect-free beryllium ion crystals using pulsed laser ablation, Rev. Sci. Instrum. **92**, 063201 (2021).

[47] D. J. Wineland, M. Barrett, J. Britton, J. Chiaverini, B. DeMarco, W. M. Itano, B. Jelenković, C. Langer, D. Leibfried, V. Meyer *et al.*, Quantum information processing with trapped ions, Philos. Trans. R. Soc. London Ser. A **361**, 1349 (2003).

[48] D. Leibfried, R. Blatt, C. Monroe, and D. Wineland, Quantum dynamics of single trapped ions, Rev. Mod. Phys. **75**, 281 (2003).

[49] G. Morigi, J. Eschner, J. I. Cirac, and P. Zoller, Laser cooling of two trapped ions: Sideband cooling beyond the Lamb-Dicke limit, Phys. Rev. A **59**, 3797 (1999).

[50] Q.-X. Mei, B.-W. Li, Y.-K. Wu, M.-L. Cai, Y. Wang, L. Yao, Z.-C. Zhou, and L.-M. Duan, Experimental Realization of the Rabi-Hubbard Model with Trapped Ions, Phys. Rev. Lett. **128**, 160504 (2022).

[51] Z. Vendeiro, J. Ramette, A. Rudelis, M. Chong, J. Sinclair, L. Stewart, A. Urvoy, and V. Vuletić, Machine-learning-accelerated Bose-Einstein condensation, Phys. Rev. Res. **4**, 043216 (2022).

[52] S. Park, M. H. Seo, R. A. Kim, and D. Cho, Motion-selective coherent population trapping by Raman sideband cooling along two paths in a Λ configuration, Phys. Rev. A **106**, 023323 (2022).

[53] V. Negnevitsky, M. Marinelli, K. K. Mehta, H.-Y. Lo, C. Flühmann, and J. P. Home, Repeated multi-qubit readout and

feedback with a mixed-species trapped-ion register, Nature (London) **563**, 527 (2018).

[54] N. Schwegler, D. Holzapfel, M. Stadler, A. Mitjans, I. Sergachev, J. Home, and D. Kienzler, Trapping and ground-state cooling of H_2^+, arXiv:2212.06456

[55] S. A. King, L. J. Spieß, P. Micke, A. Wilzewski, T. Leopold, J. R. Crespo López-Urrutia, and P. O. Schmidt, Algorithmic Ground-State Cooling of Weakly Coupled Oscillators Using Quantum Logic, Phys. Rev. X **11**, 041049 (2021).

[56] M. Brownnutt, M. Kumph, P. Rabl, and R. Blatt, Ion-trap measurements of electric-field noise near surfaces, Rev. Mod. Phys. **87**, 1419 (2015).

[57] Y. Shi, Exploring quantum information processors in NISQ era: Trapped ions and beyond (unpublished).